

Tempering of press hardening steels
PHS1500 and PHS2000: characterization
and influence on fracture toughness

Khalifa Maissara

Engineering Materials

LICENTIATE THESIS

Tempering of press hardening steels
PHS1500 and PHS2000: characterization
and influence on fracture toughness

Khalifa Maissara

Engineering Materials
Division of Materials Science
Department of Engineering Sciences and Mathematics
Luleå University of Technology

ACKNOWLEDGMENTS

I would like to thank all my supervisors, Marta-Lena Antti, Farnoosh Forouzan, Pia Åkerfeldt, and Paul Åkerström, for their invaluable support and guidance throughout this journey. I would like to thank Esa Vuorinen for his help and for the fruitful discussions. I am very thankful to Ilana Timokhina for her assistance and for being so helpful. It has been a pleasure to learn from each of you, and I deeply appreciate all that you have shared with me.

I would like to thank my friends and colleagues I have met during my time at the Division of Materials Science and at LTU; I look forward to spending more time with you. A big Thank you to Janna and Nasir for being so encouraging—I am especially grateful for our morning Fika chats. I would also like to acknowledge my colleagues from the Solid Mechanics division for being so helpful whenever needed.

A special thank you to Lars Frisk, Erik Nilsson, and Johanne Mouzon, for their technical assistance and for generously sharing their expertise.

I would like to acknowledge the financial support provided by SSAB and Scania, which made it possible for me to carry out my work within the PROCHAIN project. I am also grateful to Gestamp Hardtech AB for their technical assistance and support with the equipment essential to this research, and to the Center for High Performance Steel (CHS) for their role in administering the project.

My warmest thanks go to my beloved mother and father, as well as to my family and close friends, who have always wished the best for me and offered unwavering support throughout this time.

Luleå, December 2024

Khalifa Maissara

ABSTRACT

With the continuous development of the automobile industry, the use of advanced high-strength steel in vehicles has become increasingly prevalent. Press hardening steels, known for their ultra-high strength, are gaining significant traction in this domain. Components manufactured using press hardening exhibit high dimensional accuracy and minimal spring back. The press hardening components are produced by heating the steel blank at the austenitization temperature, followed by hot forming and rapid cooling using pressing dies. However, despite the advancement in press hardening technologies and the widespread adoption of ultra-high-strength steels, certain challenges remain in further improving the performance of these materials, particularly in understanding the effect of processing treatments.

This work studies the behavior of two ultra-high strength press hardening steels (PHS2000 and PHS1500) after undergoing heat treatment methods, specifically focusing on low-temperature tempering and press hardening. The objective is to increase the understanding of microstructure evolution and its influence on mechanical performance. The first method involved quenching the steels in oil followed by tempering at four temperatures in the range of 180-300 °C, while the second utilized die quenching to targeted temperatures, followed by air cooling to induce auto-tempering. Tensile properties, hardness, and microstructure changes were tested to understand how these treatments affect the steels' mechanical properties. The tensile properties of the steels investigated are influenced by the auto-tempering of martensite that occurs during the processes of oil quenching and die cooling. This phenomenon allows the steel to attain an optimal balance, demonstrating ultra-high strength exceeding 1900 MPa and good elongation at fracture, reaching around 8% or slightly higher. The tensile tests and microstructure analysis implied that low-temperature tempering (180-200 °C) could improve the yield strength of the steel as well as the elongation with a small reduction in the strength of the steel, in which the tempering effect caused precipitation strengthening and reducing of residual stresses in the microstructure. It was found that tempering at 300 °C promotes the formation and coarsening of cementite carbide, which led to a deterioration in the tensile elongation of the steels.

The fracture toughness and bending properties of the steels were evaluated following oil quenching, press hardening, and a combination of press hardening with subsequent bake hardening. PHS2000 displayed brittle fracture characteristics and lower fracture toughness, while PHS1500 exhibited ductile fracture behavior and higher fracture toughness, with similar trends observed in three-point bending results. STEM and EDS analyses identified precipitates of varying compositions and morphologies, with coarse precipitates acting as key factors that limit grain refinement and contribute to stress concentration, thereby influencing fracture toughness and bending properties.

CONTENTS

ACKNOWLEDGMENTS	v
ABSTRACT	vii
CONTENTS	ix
CHAPTER I: INTRODUCTION AND BACKGROUND	1
1.1 Introduction	1
1.1.1 Aim and objectives.....	2
1.1.2 Appended papers.....	3
1.2 Background.....	4
1.2.1 Press hardening process	4
1.2.2 Martensite in press hardening steels.....	5
1.2.2.1 Martensite morphology and crystallography	6
1.2.3 Tempering of martensite	9
1.2.4 Fracture toughness	10
1.2.4.1 Linear elastic fracture mechanics	11
1.2.4.2 Elastic-plastic fracture mechanics	12
a. J-integral	12
b. Crack tip opening displacement.....	13
CHAPTER II: MATERIALS AND METHODS	15
2.1 Materials.....	15
2.2 Heat treatment	16
2.3 Microstructural characterization	16
2.4 Mechanical testing	17
CHAPTER III: SUMMARY OF APPENDED PAPERS	19
3.1 Paper I.....	19
3.2 Paper II.....	19
CHAPTER IV: CONCLUSIONS AND OUTLOOK.....	21
REFERENCES	22
APPENDED PAPERS.....	27
Paper I	29
Paper II	57

CHAPTER I: INTRODUCTION AND BACKGROUND

1.1 Introduction

The implementation of new global regulations for fuel efficiency, exhaust emissions, and vehicle safety will present a big challenge to automotive makers in the upcoming decades. Numerous technologies have been developed to enhance fuel efficiency. These advancements encompass measures to improve the efficiency and performance of internal combustion engines, as well as the integration of alternative fuels and the adoption of powertrains such as electric and hybrid systems [1]. However, one of the leading approaches to improving fuel efficiency is through lightweighting. A 10% weight reduction of a passenger car can result in a 6 to 8% improvement in fuel economy and up to 6% reduction in emissions [1,2]. Lightweighting can be achieved through two strategies: optimizing the vehicle's body design or using more lightweight materials.

The structural body of a typical passenger car, known as the body in white (BiW), accounts for about 30% of the car's total weight, making it a great opportunity for lightweighting [3]. Several materials are used in the BiW structure to achieve lightweighting, such as aluminum, magnesium, and steel [4]. Steel, in particular, is a structural metallic material with significant advantages in energy efficiency and emission reduction throughout its entire life cycle. Although steel has a higher mass density compared to aluminum and magnesium, the substitution of thick low-strength steels with thin advanced high-strength steels (AHSSs) can effectively reduce its weight while maintaining structural integrity. It is crucial, however, to ensure that the use of lightweight materials does not compromise crashworthiness and occupant safety.

The continued growth of the automotive market presents an interesting opportunity for both researchers and manufacturers to innovate the next generation of steel. These advancements should enable higher strength levels while maintaining sufficient ductility and toughness to meet the standard requirements for enhanced crashworthiness and occupant safety. The attainment of a trade-off between strength and ductility/toughness presents a key challenge. This, however, can be accomplished through the application of heat treatment methods such as quenching and tempering or quenching and partitioning, as well as through the addition of carbon and other elements like niobium, nickel, and molybdenum [5–7]. Therefore, depending on the final part requirements and the sequence of manufacturing operations, tempering-related phenomena, such as stress relief annealing and paint baking, can occur. These processes are similar to low-temperature tempering in the range of 150 to 200 °C. Tailored tempering, involving elevated tempering temperatures, is also used to achieve specific properties on selected areas of the component by altering cooling histories during hot forming. Understanding the evolution of mechanical properties during

manufacturing routes is crucial for the automotive industry. Therefore, this study addresses the effect of such phenomena.

1.1.1 Aim and objectives

The aim of this work is to enhance the understanding of the microstructure evolution and its effect on mechanical performance of the recently developed press hardening steel (PHS2000) in comparison with the commonly used PHS1500 steel grade. The main objectives are:

- Investigation of the microstructural evolution in two processing routes: quenching and tempering, and press hardening.
- Study the effect of processing conditions in the two routes on tensile properties, fracture toughness, and bending.
 - Study the effect of low-temperature tempering after quenching on tensile properties and microstructure changes.
 - Study the effect of auto-tempering/bake hardening on fracture toughness and microstructure after press hardening.
- Evaluate the fracture toughness and bending properties of press hardening steels and identify the key factors that affect crack initiation and propagation.

The research questions are:

1. How do the heat treatment conditions during quenching and tempering, in comparison with press hardening, affect the microstructure and subsequent performance?
2. How do microalloying elements and heat treatments affect the microstructure, fracture toughness, and bending behavior?

1.1.2 Appended papers

Paper I: Effect of tempering on microstructure and tensile properties of ultra-high strength steels for press hardening applications

K. Maissara, F. Forouzan, P. Åkerfeldt, I. Timokhina, P. Åkerström, E. Vuorinen, M-L. Antti.

Submitted to Metallurgical and Materials Transactions A.

Paper II: Fracture toughness and bending properties of two ultra-high strength press hardened steels

K. Maissara, F. Forouzan, P. Åkerfeldt, I. Timokhina, P. Åkerström, E. Vuorinen, M-L. Antti.

To be submitted.

1.2 Background

1.2.1 Press hardening process

Press hardening, also known as hot stamping, was patented in 1974 by Norrbottens Jernverk in Luleå, a company that is currently a part of SSAB [8]. Initially, press hardening was predominantly utilized for the production of hardened components for agricultural applications [9]. However, in 1984, the technology was further developed to manufacture steel parts specifically for the automotive industry. The Saab 9000 passenger car was the first vehicle to incorporate press-hardened side impact beam parts [10]. Today, press hardening is a leading technology for producing ultra-high strength safety components used in passenger vehicles, such as A-pillars, B-pillars, bumpers, roof rails, rocker rails, and tunnel components as part of the body in white structure [11]. The use of press hardening parts not only increases passenger safety but also enables vehicle weight reduction.

There are two main process routes for press hardening: direct and indirect press hardening (Figure 1). Within the direct press hardening process, a steel blank is cut, heated up in a furnace, homogeneously austenitized at temperatures between 900-950 °C for 3 to 10 minutes. It is then transferred to a press-system for forming and quenching in a single process step (Figure 1a) [12]. On the other hand, indirect press hardening consists of a cold forming operation prior to the austenitization step, followed by hot forming of the blank to achieve the final geometry (Figure 1b). The challenges posed by high-strength steels in traditional cold forming, such as substantial springback, cracking, and reduced shape accuracy, can be effectively addressed through press hardening processes. By integrating hot forming and die quenching operations, thinner and more complicated part geometries with improved shape accuracy and diminished springback can be attained, surpassing the capabilities of cold forming processes [13,14].

In earlier implementations of the press hardening process, the blanks were typically heated in an oxygen-containing atmosphere, which could lead to oxidation and decarburization of the steel surface if the material was uncoated. This can negatively affect both the surface quality and mechanical properties of the steel parts. However, recent advancements have introduced controlled or inert atmospheres and optimized coatings, which help to mitigate these issues and may reduce the need for post-processing [1,9].

The press hardening process is associated with phase transformations. The initial microstructure of the steel before heat treatment is usually comprised of ferrite and pearlite. When the blank is transferred to the furnace and heated up to the austenitization temperature, the initial microstructure is transformed to austenite.

Subsequently, during hot forming and quenching, the microstructure undergoes an austenite-to-martensite transformation.

In the automotive industry, subsequent to the assembly of press-hardened parts onto the car's body structure, a painting operation is typically carried out on the body structure. During the painting stage, the press-hardened parts undergo a heat treatment process, usually conducted at a temperature of 140-200 °C for 20 to 90 minutes [15]. This process is similar to low-temperature tempering and is typically simulated with 20 minutes of holding at 170 °C. After the paint baking, the final mechanical properties of the components are changed; the yield strength is increased, and the ultimate tensile strength is decreased [16]. However, the martensitic structure of the steel is not greatly affected.

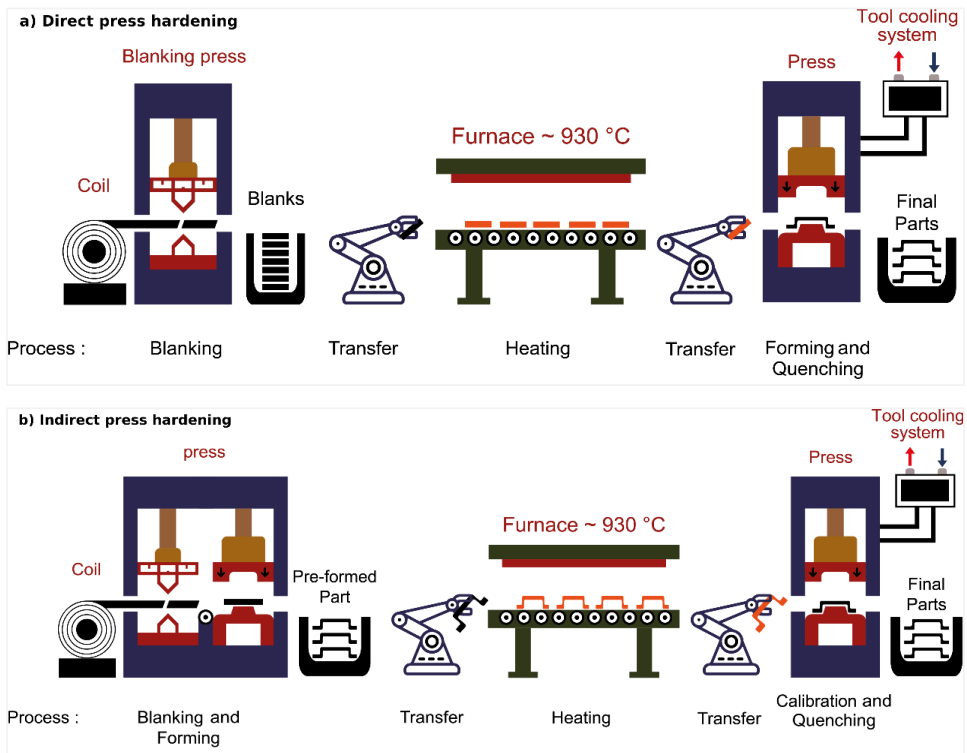


Figure 1: Schematic illustration of press hardening routes: a) direct press hardening, and b) indirect press hardening. Recreated from [12].

1.2.2 Martensite in press hardening steels

The press hardening process leads to the creation of a fully martensitic structure. A standard press-hardened part possesses a yield strength that surpasses 1000 MPa and an ultimate tensile strength of approximately 1500 MPa. Nevertheless, newly developed press-hardened steels now enable even higher strength levels, exceeding

2000 MPa. In addition to the ultra-high strength levels, the press hardening steels still retaining a good level of ductility, making them highly desirable for automotive applications. This remarkable balance of strength and ductility is due to the martensitic structure of the steel.

Martensite is generally considered to be a diffusionless transformation product resulting from the rapid cooling of austenite. In this process, the face-centered cubic (FCC) crystal structure of austenite (γ) changes to a body-centered cubic (BCC) or body-centered tetragonal (BCT) martensite, typically denoted as (α'). All grades of steel have the potential to form martensite by preventing diffusive transformations, a property known as hardenability, which is influenced by alloying elements, including carbon, chromium, manganese, and boron. In order for the martensitic transformation to take place during the rapid cooling, the Gibbs free energy of α' must be lower than that of γ ($G^{\alpha'} < G^{\gamma}$). By nature, the martensitic transformation is athermal, meaning that the volume fraction of martensite is dependent on the undercooling below the martensite start temperature (M_s). As the undercooling increases, the volume fraction of martensite also increases until it reaches approximately 100% at the martensite finish temperature (M_f). However, the M_f temperature is less distinct compared to M_s because some austenite can remain untransformed at very low temperatures, making it challenging to determine the completion of the martensite transformation. The progress of the transformation of austenite to martensite can be described by the equation of Koistinen and Marburger (equation 1) [17] as follows:

$$V_{\gamma} = \exp \{-1.10 \times 10^{-2}(M_s - T_q)\} \quad (1)$$

where V_{γ} denotes the volume fraction remaining austenite, and T_q represents the lowest temperature reached during fast cooling.

The martensitic transformation is not associated with a change in the chemical composition, meaning that the chemical composition of austenite and the transformed martensite remains unchanged. There is no diffusion of alloying elements during the transformation; however, segregation of carbon may occur, especially if the M_s is high, due to the so-called auto-tempering effect. At a macroscopic level, martensitic transformation takes place when the austenite phase deforms due to a shear stress parallel to the plane between austenite and martensite called the habit plane. This transformation is accompanied by a contraction or expansion perpendicular to the habit plane.

1.2.2.1 Martensite morphology and crystallography

Depending on the carbon content of the steel, three main martensite morphologies can be found in the form of laths, lenticular plates, or thin plates. In general, steels with carbon content higher than 0.6% will form plate martensite; on the other hand, steels with carbon content lower than 0.6 wt% will form lath martensite. Press hardening steel

grades usually contain carbon levels in the range of 0.2-0.4 wt%, falling within the lath morphology category. Consequently, the focus is directed towards lath martensite. Lath martensite forms at the highest temperatures. For example, in the case of press hardening steels, which are low alloyed steels, the M_s temperature is typically around 400 °C and M_f at 200 °C. Consequently, the steels are mostly fully martensitic at room temperature. The microstructural hierarchy of lath martensite is divided into packets, blocks, and sub-blocks, as illustrated in Figure 2. The packets are formed within a prior austenite grain and represent a collection of parallel laths with identical habit planes.

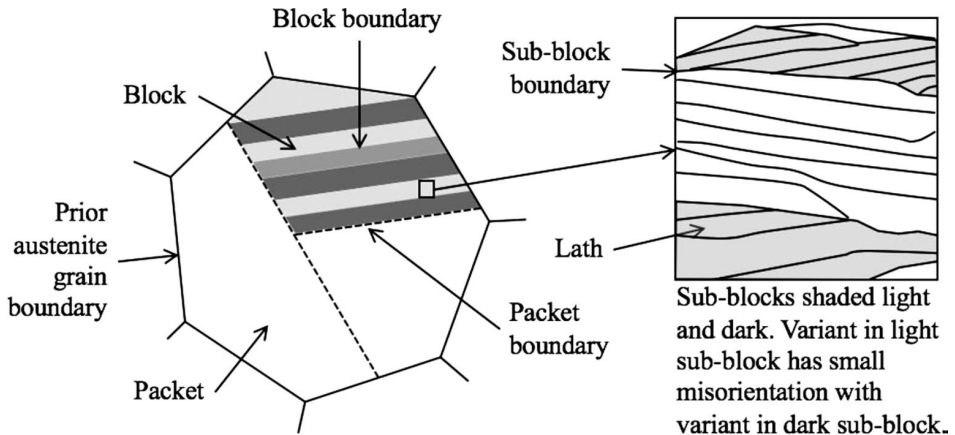


Figure 2: Schematic representation of the morphology of martensitic lath [18].

The habit plane is often used as a means of distinguishing between the different types of martensite formed in different steels or in the same steel under different conditions. This is because the habit plane changes with the carbon content and alloying content. For low carbon steels, the laths tend to lie parallel to the habit plane $\{557\}_\gamma$ [19]. It can be mentioned that the habit planes are generally *irrational*, meaning that the habit plane indices are approximate values that are close to, but not exactly $\{557\}_\gamma$.

The martensitic transformation involves the simultaneous coordinated movement of atoms over distances less than an atomic diameter. Bain was the first to propose an explanation for the atomic movement involved in the transformation of austenite to martensite. When the FCC phase transforms to BCC or BCT, the coordination number changes from 12 to 8. The coordination number refers to the number of nearest neighboring atoms surrounding a particular atom within the crystal structure. According to Bain, this change in coordination number can be visualized as straining or deforming the FCC lattice by compressing it by 18.3% along the $[001]$ direction. This compression causes the atoms to shift into BCC lattice positions, leading to an expansion of the $(001)_\gamma$ plane by 15.5% and resulting in a total volume change of approximately 3%. This deformation phenomenon is commonly referred to as the Bain strain (Figure 3).

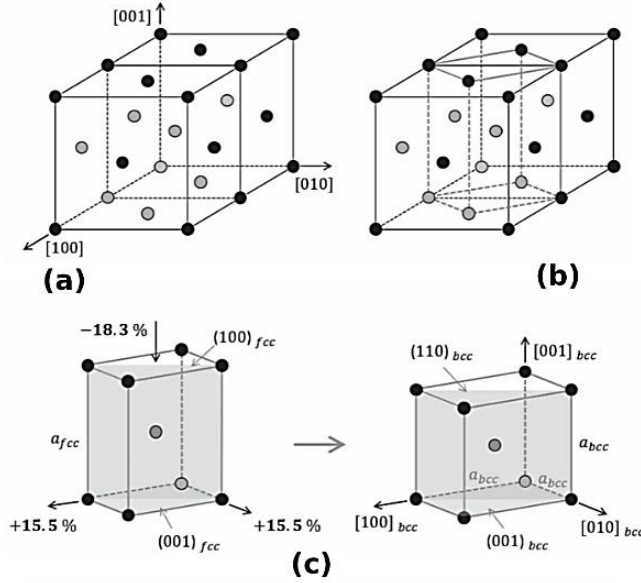


Figure 3: (a) FCC lattice forming two-unit cells. (b) a BCT unit cell in between two FCC cells. (c) a BCT to BCC transformation (Bain strain) [18].

One of the important characteristics of martensite in steels is the orientation relationship between the austenite and product martensite phases. The orientation relationship is expressed as the relationship between close-packed planes and directions in one phase with the corresponding close-packed planes and directions in the other phase. Typical austenite-martensite orientation relationships have been documented in the literature, including the well-established Kurdjumov-Sachs (K-S), Nishiyama-Wasserman (N-W), and Greninger-Troiano (G-T) orientation relationships. The low-carbon steels follow the K-S orientation relationships, which can be expressed as:

$$(111)_{\gamma} // (011)_{\alpha'} \quad [\bar{1}01]_{\gamma} // [\bar{1}\bar{1}1]_{\alpha'} \quad (\text{K-S})$$

This orientation relationship means that the close-packed plane $(111)_{\gamma}$ and direction $[\bar{1}01]_{\gamma}$ in austenite aligns parallel or nearly parallel with the close-packed plane $(011)_{\alpha'}$ and direction $[\bar{1}\bar{1}1]_{\alpha'}$ in the martensite phase, respectively. The N-W and G-T relationships are defined as follows:

$$(111)_{\gamma} // (101)_{\alpha'} \quad [1\bar{1}0]_{\gamma} \text{ 5.26}^{\circ} \text{ from } [11\bar{1}]_{\alpha'} \quad (\text{N-W})$$

$$(111)_{\gamma} // (101)_{\alpha'} \quad [1\bar{1}0]_{\gamma} \text{ 2.5}^{\circ} \text{ from } [11\bar{1}]_{\alpha'} \quad (\text{G-T})$$

In the context of the thesis, the primary function of the orientation relationships between austenite and martensite is to determine the prior austenite grain boundaries and grain size.

1.2.3 Tempering of martensite

Tempering is the process of subjecting martensitic steels to elevated temperatures, thereby inducing modifications in their microstructure and mechanical properties to suit a wide array of industrial applications. The tempering process can be conducted at temperatures ranging from as low as 150 °C, known as low-temperature tempering, to higher temperatures near the lower critical temperature of the steel, around 700 °C, which is referred to as the high-temperature tempering process. This wide temperature range provides flexibility in creating a diverse range of microstructures and mechanical properties.

Steel comprises various prominent structures, including austenite, ferrite, bainite, and martensite, each possessing distinct mechanical properties. Martensite, in particular, is valued for its ultra-high strength, making it a popular choice for industrial applications requiring high-strength steel. However, the martensitic structure is rarely used without tempering, as the internal stresses associated with the transformation can reduce the ductility of the steel. In low and medium-carbon steels, as is the case of commercial press hardening steels, the strength of the steel can exceed 2000 MPa in the as-quenched condition. Low-temperature tempering is a sufficient treatment to reduce internal stresses without changing the main structure of martensite or deteriorating the mechanical properties. The process of low-temperature tempering enhances the ductility and toughness of the as-quenched martensite while maintaining its strength and hardness at levels comparable to those of the original as-quenched state. The changes in the mechanical properties are related to the relaxation of internal stresses and precipitation of transition carbides. Within the low-temperature tempering range (150-200 °C), epsilon (ϵ)/eta (η) carbides of some nanometers in size precipitate within the martensitic crystals. This occurs as a consequence of carbon supersaturation that is relieved from the as-quenched martensite. The precipitation of transition carbides is termed the first stage of tempering. The high strength level maintained by the low-temperature tempered steels is attributed to the interaction between dislocations and the high densities of fine transition carbides. The presence of fine carbides serves as densely packed obstacles that block the motion of dislocations, leading to increased flow stresses. The annihilation of high-density dislocations has been connected with a minor increase in the total elongation of the steel [20].

Tempering just above the low-temperature tempering range results in major changes in the microstructure and the mechanical properties of the steel. This occurs within the temperature range of 200-360 °C and involves two primary phenomena: the decomposition of retained austenite to cementite (second stage of tempering) and the conversion of transition carbides into cementite (third stage of tempering) [21]. Low and medium-carbon steels usually retain a small amount of austenite after quenching. Subsequent tempering at temperatures exceeding 200 °C leads to the transformation

of the retained austenite into large cementite crystals, Fe_3C . This transformation has a detrimental effect on the toughness and ductility of the steel, ultimately leading to brittleness, a phenomenon known as tempered martensite embrittlement [22]. During the third stage of tempering, cementite nucleation primarily occurs within martensite laths, along martensite lath boundaries, and at prior austenitic grain boundaries, running in parallel with the second stage. The transition carbide within the martensite laths serves as an extra source of cementite, with cementite nucleation occurring at the eta transition carbides. The cementite grows and forms platelet shapes with $\{110\}_M$ habit planes. Major changes in the mechanical properties occur during tempering above low-temperature tempering, leading to a drop in hardness and tensile strength. This is due to coarsening within the martensitic structure, characterized by the elimination of low-angle boundaries between martensitic laths and the diffusion of carbon from the martensitic matrix into carbide precipitates.

High-temperature tempering accelerates the changes in the microstructure of martensite, leading to secondary precipitation (also known as secondary hardening) and subsequent recovery. This tempering phase, regarded as the fourth stage of tempering, is alloy-dependent. As this tempering process will not be conducted in the present study, it will not be further addressed.

Tempering is advantageous not only for preserving the strength-ductility trade-off but also for improving resistance to hydrogen embrittlement (HE). HE poses a limitation in the use of ultra-high strength steel. The hydrogen may originate from the steel processing stage or from environmental conditions like humidity and acidity during service. The HE is caused by diffusible hydrogen, which typically penetrates into the steel, diffuses to prior austenite grain boundaries, and weakens them, leading to embrittlement if a critical hydrogen concentration is reached in the steel [23]. The diffusivity of hydrogen can be controlled through microalloying with elements like Nb, V, and Ti. These microalloying elements act as traps for hydrogen, immobilizing it and thereby reducing the embrittlement effect. Compared to as-quenched martensite, tempered martensite is less susceptible to hydrogen embrittlement because as-quenched martensite is over-saturated by hydrogen [24]. Low-temperature tempering facilitates the release of diffusible hydrogen, resulting in reduced hydrogen content in steel and a corresponding decrease in its susceptibility to hydrogen embrittlement.

1.2.4 Fracture toughness

Fracture toughness is a key mechanical property that determines the material's ability to resist crack initiation and propagation. It is a crucial parameter used for designing materials for applications where catastrophic fracture is not an option, such as nuclear vessels, gas pipelines, and aircraft jet engines. Fracture toughness also plays a significant role in automotive applications due to the high demand for ultra-high strength steels, which can exhibit increased brittleness at higher strength levels. It

becomes a very important property in determining the crashworthiness of ultra-high strength steels [25,26]. The growing interest in fracture toughness for ultra-high strength steels is evident through extensive research conducted to investigate this property [27–29].

Fracture mechanics is the field that deals with catastrophic material failure resulting from the presence and propagation of a crack. Alan Griffith was the first to recognize the correlation between fracture stress and the presence of discontinuities or flaws [30]. He observed that the fracture stress of glass tension test specimens was much lower than the theoretical strength of glass. Griffith's hypothesis regarding the influence of flaws established the foundation for a novel theory of fracture in solids, introducing the concept of a size effect. This contribution helped to lay the foundation of linear elastic fracture mechanics (LEFM). Subsequently, the works of Rice [31] and Hutchinson [32] extended LEFM to non-linear problems, leading to the development of elastic-plastic fracture mechanics (EPFM).

1.2.4.1 Linear elastic fracture mechanics

LEFM is based on the basic assumption that the material fractures in a brittle manner. The basic aim of fracture mechanics was to numerically express the severity of the stress field at a crack that exists in the material. The LEFM is based on the concept of stress intensity factor (K) and assumes that only a negligible amount of plastic deformation occurs at the crack tip, making it unsuitable for more ductile materials. The stress intensity factor characterizes the crack-tip conditions in a linear elastic material and is expressed as:

$$K = Y \sigma \sqrt{\pi a} \quad (2)$$

Where Y is a geometric correction factor, σ is the applied stress, and a is a characteristic dimension of the crack.

There are three loading modes that result in high stresses at the crack tip: Mode I, Mode II, and Mode III. Mode I occurs when the applied load is perpendicular to the crack plane and is the most common mode of fracture in engineering applications, with most crack failures happening under this mode. Mode II is a sliding or shearing mode that occurs when the crack surfaces slide over each other. Mode III, known as the tearing mode, is caused by the lateral shear movement of the crack surfaces relative to each other. For these different loading modes, the stress intensity factor K is designated as K_I , K_{II} , and K_{III} .

In the context of LEFM, crack propagation occurs when the stress intensity factor (K) exceeds a critical value denoted as K_C , which represents the fracture toughness of the material. K_C varies with material thickness until a critical thickness is achieved, beyond which it becomes invariant to further changes in thickness. When this critical point is

reached, the fracture toughness is referred to as K_{IC} , representing the plane strain fracture toughness under Mode I loading.

1.2.4.2 Elastic-plastic fracture mechanics

Most materials used in engineering applications exhibit ductile behavior, in which significant plastic deformation occurs. In such materials, the application of LEFM becomes inadequate due to the large plastic zone that forms at the crack tip. To address this limitation, LEFM has been extended to account for the substantial plastic deformation, giving rise to the development of elastic-plastic fracture mechanics. The EPFM is based on the so-called J-integral and the crack-tip opening displacement (CTOD).

a. J-integral

J-integral is a key parameter in EPFM, used to characterize the fracture behavior in a component experiencing both elastic and plastic deformation. The J-integral, introduced by Rice [31], is a line integral that characterizes the energy release rate in the vicinity of a crack, particularly under conditions where significant plastic deformation occurs near the crack tip. It is path-independent, meaning that J can be determined from a stress analysis in which stress and strain are specified along any arbitrary contour surrounding a crack tip. The form of the J-integral is given in the following equation (3):

$$J = \int_C \left(W dy - T_i \frac{\partial u_i}{\partial x} ds \right) \quad (3)$$

Where W is the strain energy density, C is an arbitrary contour around the crack tip (Figure 4), T_i is the stress vector acting on the contour, u_i is the displacement vector, (x, y) are rectangular coordinates normal to the crack front, and ds is an increment of the contour C . The strain energy density is defined according to the following equation (4):

$$W = \int \sigma_{ij} d\varepsilon_{ij} \quad (4)$$

Where σ_{ij} and ε_{ij} are the stress and strain components, respectively.

In monotonic loading conditions, the crack initiates when the J-integral reaches a critical value, denoted as J_c , analogous to K_{IC} in LEFM. The critical J-integral value corresponds to the onset of stable crack propagation and provides a measure of the fracture toughness of ductile materials.

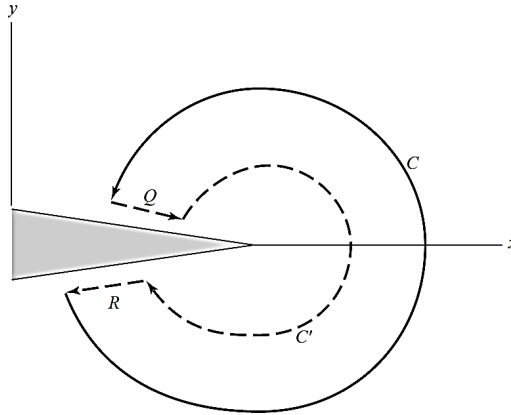


Figure 4: Arbitrary line contour surrounding the tip of a crack [33].

b. Crack tip opening displacement

The crack tip conditions in elastic-plastic materials can also be described by a parameter known as CTOD, denoted by the symbol δ . CTOD serves as a fracture criterion and was first proposed by Wells [34]. Wells observed that the plastic deformation at the crack tip caused the crack faces to move apart, causing the crack to blunt, as depicted in Figure 5. He suggested that the extent of crack tip opening could serve as a measure of fracture toughness in cases where the plastic zone near the crack tip is too large for LEFM, which led to the development of the CTOD parameter [35]. In cases of small-scale yielding, the CTOD can be related to the stress intensity factor K_I . The CTOD can be expressed as:

$$\delta = \frac{4}{\pi} \frac{K_I^2}{E \sigma_{YS}} \quad (5)$$

Where K_I is the stress intensity factor, E is the Young's modulus, and σ_{YS} is the yield strength.

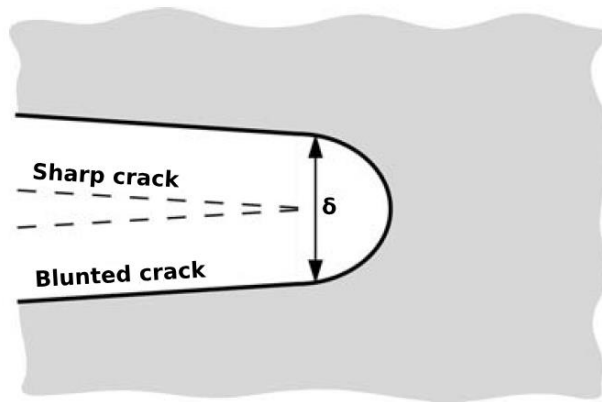


Figure 5: Crack blunting due to plastic deformation, resulting in displacement δ at the crack tip [35].

CHAPTER II: MATERIALS AND METHODS

2.1 Materials

Two different press hardening steels were investigated in this work. The first steel variant is denoted as PHS1500, while the second is referred to as PHS2000, with both produced by SSAB in Sweden. The steel sheets were received in the form of 2.5 mm thick sheets. The PHS1500 was supplied as hot rolled and the PHS2000 was supplied as hot rolled and batch annealed. The chemical compositions are listed in Table 1.

Table 1: Chemical compositions (wt.%) of the PHS1500 and PHS2000 steels.

Material	C	Si	Mn	Cr	Ti	Nb	V	W	B
PHS1500	0.246	0.271	1.223	0.215	0.035	0.001	0.006	0.011	0.0038
PHS2000	0.318	0.243	1.260	0.135	0.010	0.032	0.015	0.014	0.0013

The steel grades' continuous cooling transformation curves (CCT) were simulated using JMatPro software, which used the chemical composition of the steels and the austenitization temperature as inputs. 930 °C and 900 °C have been considered the austenitizing temperatures for PHS1500 and PHS2000, respectively. The CCT diagrams of both materials are given in Figure 6. The predicted Ms and Bs temperatures are equal to 390 and 591 °C, respectively, for the PHS1500 grade, and they are lower for the steel grade PHS2000: Ms=363 °C and Bs=582 °C. The estimated critical temperatures of both steels are summarized in Table 2. As can be estimated from the CCT diagram of PHS2000, cooling rates faster than 10 °C/s are needed in order to form a fully martensitic structure. In the case of PHS1500 material, cooling rates quicker than 20 °C/s are required to achieve a fully martensitic structure.

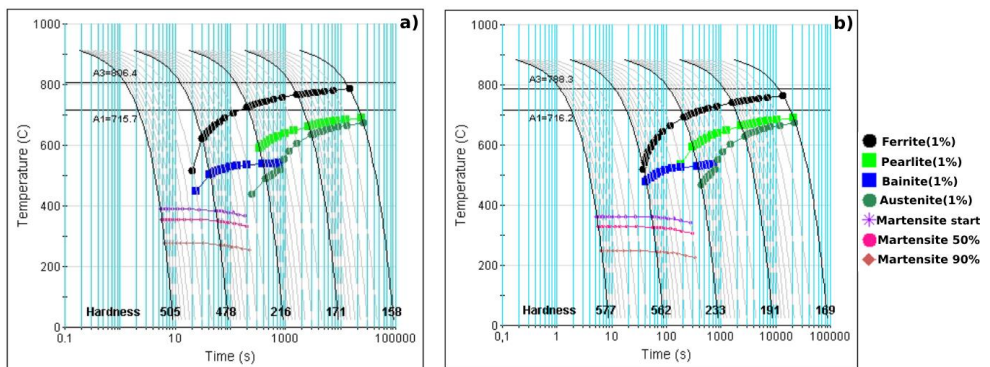


Figure 6: CCT diagrams simulated by using JMatPro software of a) PHS1500 and b) PHS2000.

Table 2: Critical temperatures (in °C) calculated using the JMatPro software.

Material	MS	Bs	A3	A1
PHS1500	390	591	806	716
PHS2000	363	582	788	716

2.2 Heat treatment

For the first study in this work, the quenching and tempering heat treatment was performed in addition to a lab-scale press hardening process. For the quenching and tempering, steels were first austenitized in a muffle furnace, quenched in oil, and then tempered at different tempering temperatures (180-300 °C) and times (2-15 min), followed by air cooling to room temperature. The lab-scale press hardening samples were austenitized and then die-quenched using a flat tool. The reader is referred to the corresponding paper (Paper I) for more details. For the second study in this work, samples from each grade were initially austenitized in a muffle furnace and then quenched in oil to room temperature. Another set of samples was austenitized and then die-quenched using a press hardening line. Furthermore, the press-hardened samples were subjected to bake hardening at 175 °C for 20 minutes to replicate the paint baking process utilized in the automotive industry. The specifics of the heat treatment process are summarized in Table 3.

Table 3: Heat treatment process parameters.

Material	Austenitization temperature (°C)	Austenitization time (s)	Cooling method	Baking temperature (°C)	Baking time (s)
PHS1500	930	300	Oil	–	–
PHS1500	930	300	Stamping die	–	–
PHS1500	930	300	Stamping die	175	1200
PHS2000	900	300	Oil	–	–
PHS2000	900	300	Stamping die	–	–
PHS2000	900	300	Stamping die	175	1200

2.3 Microstructural characterization

The microstructure was examined using light optical microscopy (OM) and scanning electron microscopy (SEM). The OM analysis was carried out using a Nikon Eclipse MA200. For the SEM investigations, a high-resolution FEI Magellan 400 was used. For

precipitate characterization, carbon extraction replicas were prepared and subsequently subjected to analysis using a scanning transmission electron microscope (STEM) housed within the FEI Magellan 400 microscope.

X-ray diffraction analysis was performed using a PANalytical AERIS tabletop XRD, equipped with a monochromator Cu-K α radiation at 40 kV and 15 mA. Data was obtained within the range of 35° to 110° at intervals of 0.01° from polished samples positioned perpendicular to the rolling direction.

2.4 Mechanical testing

The tensile properties of the heat-treated samples were evaluated using a Dartec tensile testing machine, operating at room temperature. The tensile samples were cut parallel to the rolling direction using an electrical discharge machine (EDM), and the tests were performed following the specifications outlined in the SS-EN ISO 6892-1:2019 standard.

The hardness measurements were performed using a Struers Duramin 40 microhardness tester with Vickers indenter. A load of 1 kg was employed, and the data obtained represented the average measurement derived from a minimum of ten indentations on each specimen.

The bending tests were performed in accordance with the VDA238-100 standard, with a modification made to the specimen width, reducing it from 30 mm to 20 mm. This adjustment was necessary due to the limitations of the load cell. The specimens designated for the three-point bending test were cut to the dimensions of 60x20 mm², with the bend axis aligned parallel to the rolling direction.

The fracture toughness was assessed using the compact tension C(T) specimen. The C(T) specimen's geometry is shown in Figure 7. The notch was created using electrical discharge machining (EDM) in a direction parallel to the rolling direction. A fatigue pre-crack was initiated at the tip of the notch and propagated approximately 2 mm, resulting in an initial crack size of about 10 mm, incorporating both the notch and fatigue pre-crack. A high-resolution video camera, synchronized on one side of the specimen, was utilized to monitor the crack extension. The C(T) specimens were inserted into a universal tensile testing machine and subjected to fracture, with the load vs displacement curves being recorded. J-R curves were then created for each material, following the methodology outlined in ASTM E1820 [36]. The J-R curves were used to calculate two fracture toughness parameters: J_i , the fracture toughness at cracking initiation, and $J_{0.2}$, the fracture toughness near the onset of stable crack propagation. J_i is defined as the point when the first crack extension is detected by the

video camera, while $J_{0.2}$ is obtained by the intersection of the 0.2 mm offset line with the J-R curve, in accordance with ASTM E1820.

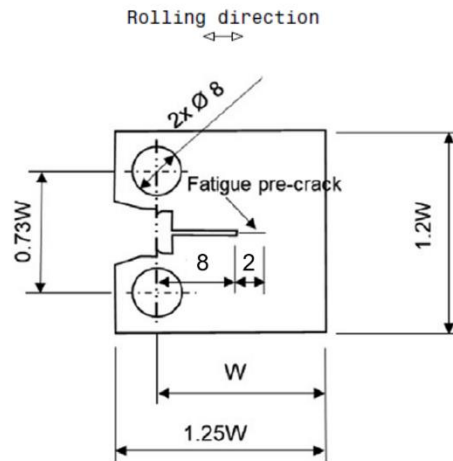


Figure 7: C(T) specimen geometry used for J-integral measurements.

CHAPTER III: SUMMARY OF APPENDED PAPERS

3.1 Paper I

Effect of tempering on microstructure and tensile properties of ultra-high strength steels for press hardening applications

Summary: This paper investigates the effect of low-tempering temperatures and auto-tempering during press hardening on the tensile properties of PHS1500 steel, which is widely used in the automotive industry for manufacturing structural components through press hardening, in comparison to PHS2000 steel, which is a new steel grade designed to boost the properties of PHS1500 in press hardening applications. This research aims to enhance the understanding of how tempering and auto-tempering affect the tensile properties and microstructure of the steel. The steels were heat-treated and tempered at four temperatures 180 °C, 200 °C, 250 °C and 300 °C. Additionally, another set of samples was press-hardened using a lab scale press equipped with planar tools to study the effect of auto-tempering during cooling. These samples were austenitized, die-quenched to various temperatures (300 °C, 200 °C, 150 °C and 100 °C), and then air-cooled. The tensile properties, hardness, microstructure, and dislocation densities after heat treatment were characterized. The results showed that tempering at 300 °C led to a drop in tensile strength and a reduction in total elongation for both steels. This was also observed for press-hardened samples when subjected to die quenching at 300 °C. The onset of this effect was observed at 250 °C. Tempering at 180 °C and 200 °C, however, resulted in improved yield strength as well as total elongation compared to the initial as-quenched state for both steels. This occurred with only a small reduction in tensile strength, making these conditions advantageous for automotive applications. The observed changes in tensile properties are driven by microstructural changes such as carbide coarsening and dislocation recovery.

Relation to thesis: In this work, research question (1) is addressed by examining the influence of quenching and tempering versus press hardening, on the evolution of microstructure and its effect on tensile performance.

3.2 Paper II

Fracture toughness and bending properties of two ultra-high strength press hardened steels

Summary: The rapid progress in the automotive market is leading to the development of new press hardening steel grades to meet the demands for improved crashworthiness and safety. Understanding the fracture resistance capabilities and controlling damage mechanisms are important to supporting this development. This

study evaluates the relationship between fracture toughness and microstructure in the recently developed ultra-high strength press hardening steel, PHS2000, and the commonly used grade, PHS1500. Additionally, the three-point bendability of these steels is investigated. Microstructure-property relationships are analyzed following a range of heat treatments, including oil quenching, press hardening, and press hardening with subsequent bake hardening. The fracture toughness after each heat treatment is evaluated in the frame of fracture mechanics using the J-integral measurements. The microstructure investigations showed that PHS1500 exhibited a finer and more uniform grain structure than PHS2000, which displayed instances of abnormal grain growth. STEM and EDS analyses identified complex carbides and carbonitrides with different morphologies. Coarse precipitates in PHS2000, containing Nb, Ti, and Mo, are likely contributors to its lower fracture toughness and bending properties, as they may act as stress concentration sites and promote microcracking. In contrast, PHS1500 showed high fracture toughness and bending properties, attributed to its refined grain structure and lower carbon content. The bake hardening treatment resulted in a slight increase in fracture toughness in PHS2000 but did not significantly improve bending performance in either steel.

Relation to thesis: In this work, research question (2) is addressed by investigating how the microalloying elements and heat treatment parameters affect the evolution of microstructure, as well as the resulting fracture toughness and bending behavior.

CHAPTER IV: CONCLUSIONS AND OUTLOOK

Oil quenching and press hardening resulted in the auto-tempering effect in the martensite microstructure. This phenomenon was observed in both steel grades, contributing to the favorable elongation properties of the as-quenched state. Notably, auto-tempering was more pronounced in PHS1500, attributed to its elevated martensite start temperature, which facilitates carbon diffusion within the pre-formed martensite. Consequently, this process yielded the formation of fine iron carbides, likely in the form of epsilon carbides. The effect of tempering temperature was more pronounced than the effect of tempering time, and a critical temperature threshold was found at 300 °C for steel performance. The tempering temperature must be carefully selected as 300 °C can lead to tempering embrittlement phenomenon due to cementite formation. Low-temperature tempering (180-200 °C) led to increased yield strength with a small reduction in ultimate tensile strength for both steels, which resulted from reducing microstructure residual stress and precipitation strengthening.

The role of microalloying elements and heat treatment parameters in controlling microstructural characteristics and mechanical performance of PHS steels offers valuable insights into the key parameters influencing fracture toughness and bending behavior. Observations of coarse precipitates, particularly in PHS2000, reveal how coarse Nb-containing particles may reduce fracture toughness and bending properties by acting as stress concentrators, and limiting the formation of finer precipitates needed for grain refinement. These findings enhance the understanding of how microstructural control in ultra-high strength steels can be optimized through careful adjustment of microalloying content and austenitization parameters to achieve a better balance of strength and toughness. Therefore, optimizing austenitization parameters to limit coarse precipitate formation while promoting finer austenite grain structures presents a promising avenue for the continuation of this work. Additionally, further characterization is needed to clarify the negligible effect of bake hardening on fracture toughness and bending properties.

REFERENCES

- [1] T. Taylor, A. Clough, Critical review of automotive hot-stamped sheet steel from an industrial perspective, *Materials Science and Technology (United Kingdom)* 34 (2018) 809–861. <https://doi.org/10.1080/02670836.2018.1425239>.
- [2] M. Kiani, I. Gandikota, M. Rais-Rohani, K. Motoyama, Design of lightweight magnesium car body structure under crash and vibration constraints, *Journal of Magnesium and Alloys* 2 (2014) 99–108. <https://doi.org/10.1016/j.jma.2014.05.005>.
- [3] S.A. Pradeep, R.K. Iyer, H. Kazan, S. Pilla, Automotive Applications of Plastics: Past, Present, and Future, in: *Applied Plastics Engineering Handbook: Processing, Materials, and Applications: Second Edition*, Elsevier Inc., 2017: pp. 651–673. <https://doi.org/10.1016/B978-0-323-39040-8.00031-6>.
- [4] A. Kelkar, R. Roth, J. Clark, Automobile Bodies: Can Aluminum Be an Economical Alternative to Steel?, *Automotive Materials* 53 (2001) 28–32. <https://doi.org/https://doi.org/10.1007/s11837-001-0131-7>.
- [5] S. shuo Li, H. wen Luo, Medium-Mn steels for hot forming application in the automotive industry, *International Journal of Minerals, Metallurgy and Materials* 28 (2021) 741–753. <https://doi.org/10.1007/s12613-020-2179-9>.
- [6] J. Yoo, M.C. Jo, J. Bian, S.S. Sohn, S. Lee, Effects of Nb or (Nb + Mo) alloying on Charpy impact, bending, and delayed fracture properties in 1.9-GPa-grade press hardening steels, *Mater Charact* 176 (2021). <https://doi.org/10.1016/j.matchar.2021.111133>.
- [7] T. Taylor, G. Fournalis, A. Clough, Effect of carbon and microalloy additions on hot-stamped boron steel, *Materials Science and Technology (United Kingdom)* 33 (2017) 1964–1977. <https://doi.org/10.1080/02670836.2017.1342018>.
- [8] G. Berglund, The history of hardening of boron steel in northern Sweden, in: K. Steinhoff, M. Oldenburg, B. Prakash (Eds.), *1st International Conference on Hot Sheet Metal Forming of High-Performance Steel*, Kassel, 2008: pp. 175–177.
- [9] D.W. Fan, B.C. De Cooman, State-of-the-knowledge on coating systems for hot stamped parts, *Steel Res Int* 83 (2012) 412–433. <https://doi.org/10.1002/srin.201100292>.
- [10] L.M. Arias, G. Artola, I. Porto, Hot Stamping Research Scenarios from the Last Decade, in: MDPI AG, 2021: p. 26. <https://doi.org/10.3390/iec2m-09245>.
- [11] H. Karbasian, A.E. Tekkaya, A review on hot stamping, *J Mater Process Technol* 210 (2010) 2103–2118. <https://doi.org/10.1016/j.jmatprotec.2010.07.019>.

- [12] Hot Stamping of Ultra High-Strength Steels, Springer International Publishing, 2019. <https://doi.org/10.1007/978-3-319-98870-2>.
- [13] Z. Cheng, M. Gao, J. Liu, S. Wang, G. Wu, J. Gao, H. Wu, X. Mao, Multi-Scale Microstructural Tailoring and Associated Properties of Press-Hardened Steels: A Review, *Materials* 16 (2023). <https://doi.org/10.3390/ma16103799>.
- [14] K. Mori, P.F. Bariani, B.A. Behrens, A. Brosius, S. Bruschi, T. Maeno, M. Merklein, J. Yanagimoto, Hot stamping of ultra-high strength steel parts, *CIRP Ann Manuf Technol* 66 (2017) 755–777. <https://doi.org/10.1016/j.cirp.2017.05.007>.
- [15] W. Bleck, S. Bruhl, T. Gerber, A. Katsamas, R. Ottaviani, L. Samek, S. Traint, Control and exploitation of the bake-hardening effect in multi-phase high-strength steels, 2007. http://ec.europa.eu/research/rtdinfo/index_en.html.
- [16] H. Järvinen, M. Honkanen, M. Järvenpää, P. Peura, Effect of paint baking treatment on the properties of press hardened boron steels, *J Mater Process Technol* 252 (2018) 90–104. <https://doi.org/10.1016/j.jmatprotec.2017.08.027>.
- [17] J.S. Erickson, J.R. Low, A general equation prescribing the extent of the austenite-martensite transformation in pure iron-carbon alloys and plain carbon steels, *Acta Metallurgica* 7 (1959) 59–60.
- [18] D.A. Porter, K.E. Easterling, M.Y. Sherif, *Phase Transformations in Metals and Alloys*, 4th ed., 2022.
- [19] E. Pereloma, D. V Edmonds, Crystallography of martensite transformations in steels, in: *Phase Transformations in Steels*, 2012. <https://doi.org/https://doi.org/10.1533/9780857096111.1.3>.
- [20] M. Naderi, M. Abbasi, A. Saeed-Akbari, Enhanced mechanical properties of a hot-stamped advanced high-strength steel via tempering treatment, *Metall Mater Trans A Phys Metall Mater Sci* 44 (2013) 1852–1861. <https://doi.org/10.1007/s11661-012-1546-1>.
- [21] L. Cheng, C.M. Brakman, B.M. Korevaar, E.J. Mittemeijer, The Tempering of Iron-Carbon Martensite; Dilatometric and Calorimetric Analysis, *METALLURGICAL TRANSACTIONS A* 19A (1988).
- [22] G. Krauss, Tempering of martensite in carbon steels, in: E. Pereloma, D. V Edmonds (Eds.), *Phase Transformations in Steels Diffusionless Transformations, High Strength Steels, Modelling and Advanced Analytical Techniques*, Woodhead Publishing Series in Metals and Surface Engineering, 2012: pp. 126–150.
- [23] B. Jian, L. Wang, H. Mohrbacher, H.Z. Lu, W.J. Wang, Development of Niobium Alloyed Press Hardening Steel with Improved Properties for Crash Performance,

- Adv Mat Res 1063 (2014) 7–20.
<https://doi.org/10.4028/www.scientific.net/amr.1063.7>.
- [24] C. Georges, T. Sturel, P. Drillet, J.M. Mataigne, Absorption/desorption of diffusible hydrogen in aluminized boron steel, *ISIJ International* 53 (2013) 1295–1304.
<https://doi.org/10.2355/isijinternational.53.1295>.
- [25] D. Frómeta, A. Lara, S. Molas, D. Casellas, J. Rehrl, C. Suppan, P. Larour, J. Calvo, On the correlation between fracture toughness and crash resistance of advanced high strength steels, *Eng Fract Mech* 205 (2019) 319–332.
<https://doi.org/10.1016/j.engfracmech.2018.10.005>.
- [26] D. Casellas, A. Lara, D. Frómeta, D. Gutiérrez, S. Molas, L. Pérez, J. Rehrl, C. Suppan, Fracture Toughness to Understand Stretch-Flangeability and Edge Cracking Resistance in AHSS, *Metall Mater Trans A Phys Metall Mater Sci* 48 (2017) 86–94. <https://doi.org/10.1007/s11661-016-3815-x>.
- [27] D. Frómeta, S. Parareda, A. Lara, S. Molas, D. Casellas, P. Jonsén, J. Calvo, Identification of fracture toughness parameters to understand the fracture resistance of advanced high strength sheet steels, *Eng Fract Mech* 229 (2020).
<https://doi.org/10.1016/j.engfracmech.2020.106949>.
- [28] S. Golling, D. Frómeta, D. Casellas, P. Jonsén, Influence of microstructure on the fracture toughness of hot stamped boron steel, *Materials Science and Engineering: A* 743 (2019) 529–539.
<https://doi.org/10.1016/j.msea.2018.11.080>.
- [29] Q. Lai, Z. Chen, Y. Wei, Q. Lu, Y. Ma, J. Wang, G. Fan, Towards the understanding of fracture resistance of an ultrahigh-strength martensitic press-hardened steel, *Journal of Materials Research and Technology* 27 (2023) 1996–2006.
<https://doi.org/10.1016/j.jmrt.2023.10.090>.
- [30] E.E. Gdoutos, *Solid Mechanics and Its Applications*, n.d.
<http://www.springer.com/series/6557>.
- [31] J.R. Rice, *A Path Independent Integral and the Approximate Analysis of Strain Concentration by Notches and Cracks*, 1968.
- [32] J.R. Rice, G.F. Rosengren, Plane strain deformation near a crack tip in a power-law hardening material, *J. Me&. Phys. Solids* 16 (1968) 1–12.
- [33] D. Francois, A. Pineau, A. Zaoui, *Mechanical Behaviour of Materials*, 2013.
<http://www.springer.com/series/6557>.

REFERENCES

- [34] X.K. Zhu, J.A. Joyce, Review of fracture toughness (G, K, J, CTOD, CTOA) testing and standardization, *Eng Fract Mech* 85 (2012) 1–46. <https://doi.org/10.1016/j.engfracmech.2012.02.001>.
- [35] T.L. Anderson, *Fracture mechanics fundamentals and applications*, 3rd ed., 2005.
- [36] ASTM E1820, *Standard Test Method for Measurement of Fracture Toughness*, American Society for Testing and Materials (n.d.). <https://doi.org/10.1520/E1820-13>.

Department of Engineering Sciences and Mathematics
Division of Materials Science

ISSN 1402-1757

ISBN 978-91-8048-694-1 (print)

ISBN 978-91-8048-695-8 (pdf)

Luleå University of Technology 2024

